PHYSICAL REVIEW B **78**, 201403(R) (2008)

Plasmon dispersion and damping in electrically isolated two-dimensional charge sheets

Yu Liu and R. F. Willis
Department of Physics, The Pennsylvania State University, University Park, Pennsylvania 16802, USA

K. V. Emtsev and Th. Seyller
Lehrstuhl für Technische Physik, Universität Erlangen-Nürnberg, Nürnberg 91058, Germany
(Received 1 February 2008; published 5 November 2008)

Using high-resolution reflection electron-energy-loss spectroscopy (HREELS), we compare experimental results for the wave-vector-dependent behavior of plasmons in a graphene sheet on SiC(0001) with that due to a filled band of surface states on semiconducting silicon. There are significant differences in behavior between the two systems and the behavior predicted for a classical two-dimensional sheet of electrons. In particular, the damping increases with wave vector independent of any obvious inelastic scattering channel. The results illustrate the importance of finite-momentum, nonlocal potential effects for the dynamical behavior of electrically isolated charge sheets.

DOI: 10.1103/PhysRevB.78.201403 PACS number(s): 73.20.Mf, 71.45.Gm, 73.61.Wp

The electronic properties of graphene, a two-dimensional (2D) monolayer of carbon atoms connected in a honeycomb lattice, have become the subject of much experimental and theoretical interest[1] since it became practical to produce single sheets of this graphitic material.[2] This is due to a unique characteristic of the dispersion of its π bands, which meet at a single symmetry point, the K point of a hexagonal Brillouin zone.[3] In conventional 2D electron-gas systems, in which charge is trapped in semiconductor inversion layers,[4] heterostructure,[5] or surface states,[6] the single-particle energy $E(k)$ varies with the momentum k quadratically in parabolic bands at the Fermi energy, E_F. In graphene, the charge carriers propagate in π states which are linear through E_F with energies, $E=|\hbar k|v_F$ ($\hbar$-reduced Planck's constant) and extremely high Fermi velocity, $v_F \sim 1/300c$ (c=speed of light). The effective mass, $m^*=\hbar k_F/v_F$, is much lower than that of particles in a parabolic band, such that electron-electron collisions are more likely to occur, creating conditions for intriguing relativistic electrodynamics in a weakly interacting 2D electron system.[7]

We report experimental results for the wave-vector-dependent behavior of the frequency of the two-dimensional π plasmon, $\omega_\pi(q)$, a collective oscillation of the π-band charge density which propagates within the graphene sheet. This low-energy "sheet-plasmon" mode is different from the bulk π-plasmon mode, which is a collective excitation of the π-valence electrons in bulk graphite.[8] The graphene π-plasmon mode is a strictly 2D mode whose energy decreases continuously to zero in the long wavelength (classical) limit $q \to 0$. Recent calculations of the dynamical dielectric function $\epsilon(q,\omega)$ (Ref. 9) indicate that the 2D graphene polarizability is very different from that of systems studied to date with parabolic band dispersion.[10] Accordingly, in this Rapid Communication we compare and contrast the "sheet-plasmon" dispersion and lifetime characteristics of graphene on SiC(0001) with that of a 2D electron gas, of similar charge density $n \sim 10^{13}$ free-carriers cm^{-2}, trapped in a surface state on semiconducting silicon.[6] In both cases, the 2D charge layer is isolated from its substrate charge by a charge inversion layer and Schottky potential barrier. The reduced screening of the sheet-charge electric field produces strong nonlocal field effects, increasing with increasing wave vector q.[11] In the case of graphene, the onset of Landau damping is not observed at $q \sim k_F$, the sheet plasmon continuing to disperse at large wave vectors, $q > k_F$.

A single layer of graphene was prepared on a 6H-SiC(0001) crystalline wafer surface (0.1 Ω cm resistivity) by solid-state graphitization.[12] The sheet structure has been well characterized as weakly coupled to the substrate SiC, floating on a carbon-rich $(6\sqrt{3}\times 6\sqrt{3})R30°$ interfacial superstructure.[13,14] As a comparison, a 2D electron gas of the same charge density was prepared by first depositing one monolayer of silver atom onto a Si(111)-(7×7) reconstructed surface of an n-type silicon wafer (15 Ω cm resistivity) to form Si(111)-$(\sqrt{3}\times\sqrt{3})R30°$-Ag and following certain silver adatom deposition at elevated temperature around 600 K. Measurements were performed in ultrahigh vacuum (2×10^{-10} Torr base pressure), using a high-resolution angle-resolved reflection electron-energy-loss spectrometer (HREELS) with a setting of medium energy resolution of ~10 meV to obtain a strong signal. The momentum (slit) resolution is better than 0.01 Å^{-1}.[15]

Figure 1 shows the energy-loss peak in the HREELS spectrum of low-energy electrons backscattered from graphene on SiC(0001), increasing and dispersing with increasing momentum transfer parallel to the surface q given in Å^{-1}. All data are shown for positive momentum transfer at 300 K. Comparing with dramatic energy dispersion (0.2 ~2 eV), the nondispersing low loss peaks P1 (~67 meV) and P2 (~159 meV) were superimposed on the background and sheet-plasmon peak loss profile. They become visible as the steep intensity drop at increasing off-specular angle θ_s. Peak P1 was reported previously in the HREELS study of graphitic surface as low-energy π plasmon.[16,17] Also the peak P2 originates from Fuchs-Kliewer (FK) optical phonons of both graphitic structures on the SiC substrate[17,18] and SiC surface itself.[19,20]

In Fig. 2, the relative intensity of the sheet-plasmon loss peak increases at small momentum transfer $q \leq 0.05$ Å^{-1} before decreasing at larger $q > 0.05$ Å^{-1}. This small-angle scattering is characteristic of dipole scattering coupling to an image-charge electric field [Eq. (2)] predominantly normal to

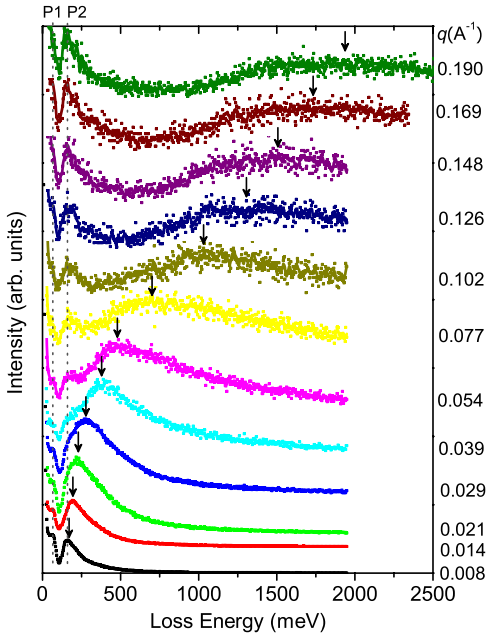

FIG. 1. (Color online) Sheet-plasmon loss peaks of graphene dispersing with increasing momentum transfer q. The lines in magnified spectra at large momentum transfer (>0.5 Å^{-1}) are smoothed by averaging 3–5 nearest-neighbor points. The incident electron-beam energy is 20.29 eV.

the 2D-sheet surface plane.[21] Information on the sheet-plasmon collective excitations is given by the imaginary part of the surface response function,[22]

$$g(q,\omega) = \int d\vec{r} \int d\vec{r}' e^{q\cdot z} \chi(\vec{r},\vec{r}',\omega) V_{\text{ext}}(\vec{r}',\omega), \qquad (1)$$

where the external "image-charge potential" has the form

$$V_{\text{ext}}(\vec{r}',\omega) = -\frac{2\pi}{q} e^{q\cdot z} e^{iq\cdot r} e^{i\omega t} \qquad (2)$$

for wave vector q and position vector r in the sheet plane ($z=0$) of excitations with energy loss, $E=\hbar\omega$. The polarizability is expressed by the frequency-dependent charge-density response function $\chi(\vec{r},\vec{r}',\omega)$, the imaginary part of which is a peak in the recorded energy-loss spectrum.[23] The loss peak, Fig. 1, sits on a Drude background continuum of single-particle excitations (SPEs), which has an analytical form[16]

$$f(x) = a(x-x_0) + b + c(x-x_0)^{-1} + d(x-x_0)^{-2} + \ldots, \qquad (3)$$

where the spectrum intensity, $f(x)$, is the function of energy x, and a,b,c,d,x_0 are coefficients to extrapolate the spectrum background. Subtraction of this background gives the loss-peak position as plasmon energy plotted in Fig. 3.

The Fermi energy of the graphene layer is raised 0.57 eV above the Dirac-energy crossing point of the π bands, with $k_F \sim 0.08$ Å^{-1} corresponding to a 2D charge density $n \sim 2 \times 10^{13}$ cm^{-2}. The Fermi level is pinned within the ~ 3 eV bulk band gap of the substrate and effectively decoupled from charge excitations in the substrate.[24]

Figure 3 compares the dispersion behaviors of the plasmon losses observed in the HREELS spectra from both surfaces. The data for the sheet plasmon due to a metallic surface-state band in the band gap of the silicon substrate, Fig. 3(b), are in agreement with published data.[6] The different band structures (inset diagrams) produce different distributions of SPEs, plotted for both cases, Fig. 3, in relation to the $\sqrt{q}$ dispersion predicted for a 2D charge sheet of free electrons of the same number density. The first thing we note is that the plasmons in both cases have exactly the same $\sqrt{q}$ dispersion as that for a classical 2D electron gas in the local-field approximation in the long wavelength limit.[25] Stern[26] expressed this, and higher-order, nonlocal field effects in a random-phase approximation:

$$\omega_{2D} = \left[\frac{4\pi n e^2}{m^*(1+\epsilon_0)} |q| + \frac{3}{4} v_F^2 q^2 + \cdots \right]^{1/2}. \qquad (4)$$

The first term (indicated by blue dashed lines, Fig. 3) is dependent on the areal charge density n, effective mass m^*, and static dielectric constant ϵ_0 of the medium. The Fermi momentum and the Fermi energy of graphene are given by $k_F = (4\pi n / g_s g_v)^{1/2}$ and $E_F = \hbar v_F k_F$, where $g_s=2$ and $g_v=2$ are the spin and valley degeneracies for graphene.[9] The data for graphene have only one best-fit parameter: effective mass $m^* = 0.077 m_e$ where a constant value $\epsilon_0 = 10$ for SiC and $n = 1.9 \times 10^{13}$ cm^{-2} from photoemission measurements are used in fitting. The data for the 2D surface state on Si(111)-$(\sqrt{3}\times\sqrt{3})R30°$-Ag were fitted in the same way in Ref. 6, giving $n = 1.9 \times 10^{13}$ cm^{-2} and $m^* = 0.24 m_e$ with a constant value $\epsilon_0 = 11.5$ for silicon.[27]

The second thing we note is that even though the long wavelength plasmons have almost identical dispersion at small q, the data deviate strongly from $\sqrt{q}$-dispersion behavior with increasing finite q. Also, this deviation is different in the graphene, the data falling below the $\sqrt{q}$ curve for $0.1 \leq q/k_F \leq 0.5$, while that for the 2D surface state shows an increasing plasmon energy, E_{loss}, relative to the Fermi energy, E_F, in Fig. 3. This behavior is surprising, given Stern's result [Eq. (4)] for the dispersion of a 2D electron gas within RPA, including finite wave-vector nonlocal higher-order corrections. Equation (4) expresses the first-order correction in

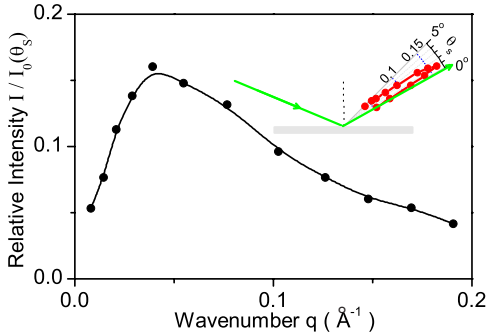

FIG. 2. (Color online) Scattering cross-section intensity varying with q. The angular distribution profile (inset diagram, red line) of loss intensity is strongly peaked around 1.5° to specular direction (green line). Scattering angle ($0° \leq \theta_s < 5°$) is magnified by three times in polar coordinates to ensure visibility.

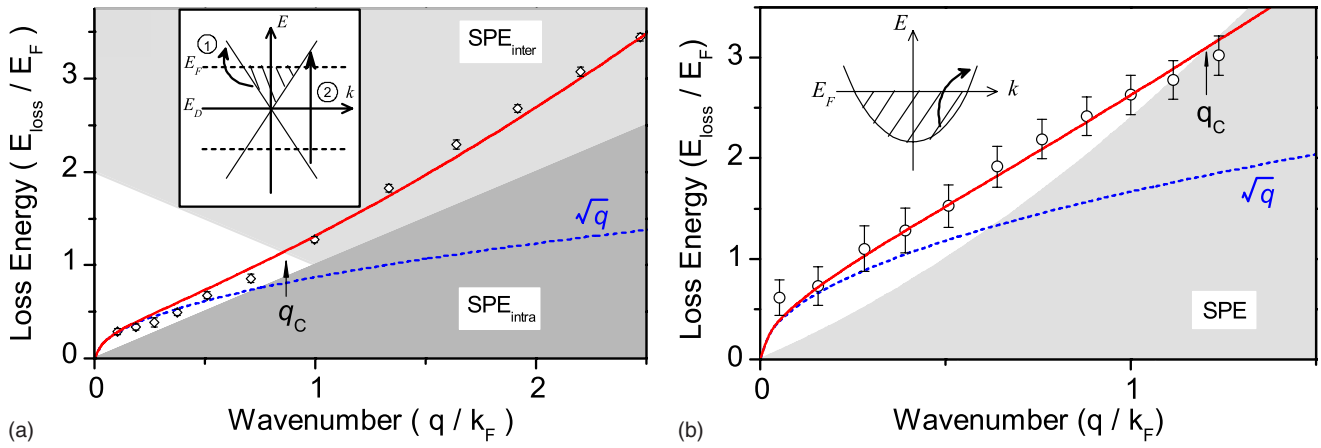

FIG. 3. (Color online) Plasmon dispersion for (a) graphene of similar charge density, (E_F=0.57 eV) $n \sim 2\times10^{13}$ cm^{-2} and (b) Si(111)-($\sqrt{3}\times\sqrt{3}$)$R30°$-Ag surface-state band (E_F=0.19 eV), $n \sim 2\times10^{13}$ cm^{-2}. The respective band structures (inset diagrams) show the origin of SPEs (1) intraband and (2) interband. Graphene is ambipolar with electron and hole carriers in separate π, π^* bands. q_c indicates the onset where plasmon enters the damping region. The blue dashed curves correspond to $\sqrt{q}$ dispersion of free 2D electron gas with the same electron density, and the red full curves correspond to best fits to experimental results.

terms of the Fermi velocity v_F, which is at least an order of magnitude smaller in the 2D surface-state band.

Hwang and Das Sarma[9] have recently shown that the wave-vector-dependent dynamical polarizability of graphene can be expressed as

$$\epsilon(q,\omega) = 1 + \nu_c(q)\Pi(q,\omega), \tag{5}$$

in which the 2D screened Coulomb interaction, $\nu_c(q) = 2\pi e^2/\kappa q$, and κ is an effective dielectric constant in which dynamical screening effects are absorbed into the static constant ϵ_0. The 2D dynamic polarizability is the sum of two terms representing the ambipolar nature of the free carriers in "doped" graphene [inset diagram, Fig. 3(a)]:

$$\Pi(q,\omega) = \Pi^+(q,\omega) + \Pi^-(q,\omega), \tag{6}$$

with Π^+, Π^- representing the polarizability of the hole gas and electrons excited up into the π^* states.

Hwang's prediction of the plasmon dispersion is borne out by the experimental results [Fig. 3(a)]. The nonlocal polarization of the hole band in graphene reduces the plasmon frequency below that of the classical 2D electron gas for $q < 0.5k_F$. There is no such depolarization effect in the 2D surface-state system; see Fig. 3(b). The nonlocal effects produce a well-established increase in the plasmon frequency at larger q.[28] With increasing wave vector, $q > k_F$, we see a third difference in behavior between the graphene and the 2D surface state. In Fig. 3, we show also the onset of the continuum dispersion of SPEs throughout (q,ω) space (shaded regions). The plasmon in the surface-state system, Fig. 3(b), disappears into the continuum of intraband transitions at $q_c \sim 0.14$ Å^{-1} beyond which point it dissolves into incoherent electron-hole pairs which form a continuum Drude background of energy-loss excitations. In contrast, the graphene plasmons, Fig. 3(a), avoid the linear SPE edge due to intraband excitations, entering the continuum of interband excitations at $q_c \sim 0.08$ Å^{-1} [the different energy scales of the intra- and interband excitations are illustrated on the band diagram inset; see Fig. 3(a)]. However, all of the spectral weight of the graphene mode is not transferred to the inter-SPEs, the 2D π plasmon continuing to disperse at higher $q > k_F$.

Another surprising feature of both dispersing plasmon modes is an increasing lifetime broadening even within the energy gap of SPEs. Figure 4 compares the observed change of this damping with increasing finite q for these two systems. Both curves show a linear increase in the plasmon damping with increasing wave vector q. The slopes of the curves are roughly in the ratio of their Fermi velocities: v_F(graphene)/v_F(surface state)=$(1.1\times10^6$ m/s)/$(5.3\times10^5$ m/s)~ 2.08. This peculiar nature of the plasmon damping is a consequence of the restricted phase space for scattering and reduced screening due to the absence of substrate excitations. Damping due to collisions with phonons does not conserve momentum, and the growth in damping has been shown to be temperature independent.[6,9] A similar effect has also been reported for a 2D electron gas formed in a GaAs/AlGaAs quantum well as evidence for enhanced correlation effects.[5] Another contribution factor is the small magnitude of $k_F \sim 0.08$ Å^{-1}, giving plasmon wavelengths $\lambda_p \sim 70$ Å, which are large compared with the lattice size

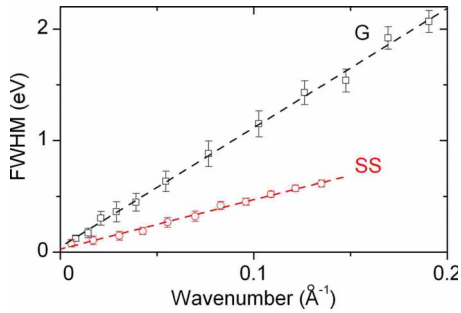

FIG. 4. (Color online) Plasmon damping [full width at half maximum (FWHM) of loss peak, Fig. 1] plotted as a function of momentum transfer q for (G) graphene and (SS) surface-state 2D systems.

$a \sim 1.5$ Å. These sheet plasmons do not scatter off the lattice.

In conclusion, we find a number of intriguing differences between the sheet-plasmon behavior of a sheet of charge effectively isolated from screening by substrate excitations. These differences are manifest with increasing wave vector q, and have been widely predicted as due to nonlocal corrections.[5,9,11] These nonlocal corrections effectively increase the restoring force (potential) of the plasmon harmonic oscillator, and contribute to damping increasing with q irrespective of Landau damping due to excitations of single-particle, electron-hole pairs on the Fermi surface. These effects are magnified in graphene due to the very limited amount of phase space available to electron scattering processes, and the increased electron-electron elastic scattering due to the very high Fermi velocity v_F. The dynamical screening behavior is, as a consequence, very different from that of the usual 2D electron gas.

Y.L. and R.F.W. thank the Petroleum Research Fund of the American Chemical Society for funding this research under Grant No. 43557-AC5. K.V.E. and Th.S. acknowledge funding by the Deutsche Forschungsgemeinschaft under Grant No. SE1087/5-1.

[1] A. K. Geim and K. S. Novoselov, Nature Mater. **6**, 183 (2007).
[2] H. Shioyama, J. Mater. Sci. Lett. **20**, 499 (2001).
[3] B. Partoens and F. M. Peeters, Phys. Rev. B **74**, 075404 (2006).
[4] S. J. Allen, D. C. Tsui, and R. A. Logan, Phys. Rev. Lett. **38**, 980 (1977).
[5] C. F. Hirjibehedin, A. Pinczuk, B. S. Dennis, L. N. Pfeiffer, and K. W. West, Phys. Rev. B **65**, 161309(R) (2002).
[6] T. Nagao, T. Hildebrandt, M. Henzler, and S. Hasegawa, Phys. Rev. Lett. **86**, 5747 (2001).
[7] M. Wilson, Phys. Today **59**(1), 21 (2006).
[8] T. Pichler, M. Knupfer, M. S. Golden, J. Fink, A. Rinzler, and R. E. Smalley, Phys. Rev. Lett. **80**, 4729 (1998).
[9] E. H. Hwang and S. Das Sarma, Phys. Rev. B **75**, 205418 (2007).
[10] V. M. Silkin, A. García-Lekue, J. M. Pitarke, E. V. Chulkov, E. Zaremba, and P. M. Echenique, Europhys. Lett. **66**, 260 (2004).
[11] T. Inaoka, T. Nagao, S. Hasegawa, T. Hildebrandt, and M. Henzler, Phys. Rev. B **66**, 245320 (2002).
[12] I. Forbeaux, J.-M. Themlin, and J.-M. Debever, Phys. Rev. B **58**, 16396 (1998).
[13] A. Bostwick, T. Ohta, T. Seyller, K. Horn, and E. Rotenberg, Nat. Phys. **3**, 36 (2007).
[14] K. Emtsev, T. Seyller, F. Speck, L. Ley, P. Stojanov, J. Riley, and R. Leckey, Mater. Sci. Forum **556**, 525 (2007).
[15] The Instrument was a commercial LK2000-14-R spectrometer (LK industries) with reconfigured narrow slits.
[16] P. Laitenberger and R. E. Palmer, Phys. Rev. Lett. **76**, 1952 (1996).
[17] T. Angot, M. Portail, I. Forbeaux, and J. M. Layet, Surf. Sci. **502–503**, 81 (2002).
[18] W.-H. Soe, K.-H. Rieder, A. M. Shikin, V. Mozhaiskii, A. Varykhalov, and O. Rader, Phys. Rev. B **70**, 115421 (2004).
[19] T. Balster, F. Tautz, V. Polyakov, H. Ibach, S. Sloboshanin, R. Öttking, and J. Schaefer, Surf. Sci. **600**, 2886 (2006).
[20] V. van Elsbergen, H. Nienhaus, and W. Mönch, Appl. Surf. Sci. **123–124**, 38 (1998).
[21] D. M. Newns in *Vibrational Spectroscopy of Adsorbates*, edited by R. F. Willis (Springer-Verlag, New York, 1980).
[22] M. Rocca, Surf. Sci. Rep. **22**, 1 (1995).
[23] A. Liebsch, *Electronic Excitations at Metal Surfaces* (Plenum, London, 1997).
[24] T. Seyller, K. Emtsev, F. Speck, K.-Y. Gao, and L. Ley, Appl. Phys. Lett. **88**, 242103 (2006).
[25] N. H. March and M. P. Tosi, Adv. Phys. **44**, 299 (1995).
[26] F. Stern, Phys. Rev. Lett. **18**, 546 (1967).
[27] The extrapolation to origin of the best-fit curve (red lines in Fig. 3) is required by 2D electron-gas theory (Refs. 9 and 26). To experimentally characterize behaviors in the region $q \rightarrow 0$ Å^{-1}, optical experiments are necessary due to the inaccessibility to that region by HREELS.
[28] A. Yurtsever, V. Moldoveanu, and B. Tanatar, Phys. Rev. B **67**, 115308 (2003).